Rapid Communications

Dynamic x-ray diffraction and nanosecond quantification of kinetics of formation of β-zirconium under shock compression

Patricia Kalita,* Justin Brown, Paul Specht, and Seth Root
Sandia National Laboratories, Albuquerque, New Mexico 87125, USA

Melanie White
Dept. of Physics, University of Nevada Las Vegas, Las Vegas, Nevada 89154, USA

Jesse S. Smith
High-Pressure Collaborative Access Team, X-ray Science Division, Argonne National Laboratory, Argonne, Illinois 60439, USA

(Received 7 October 2019; revised 30 June 2020; accepted 6 July 2020; published 3 August 2020)

We report the atomic- and nanosecond-scale quantification of kinetics of a shock-driven phase transition in Zr metal. We uniquely make use of a multiple shock-and-release loading pathway to shock Zr into the β phase and to create a quasisteady pressure and temperature state shortly after. Coupling shock loading with *in situ* time-resolved synchrotron x-ray diffraction, we probe the structural transformation of Zr in the steady state. Our results provide a quantified expression of kinetics of formation of β-Zr phase under shock loading: transition incubation time, completion time, and crystallization rate.

DOI: 10.1103/PhysRevB.102.060101

A leading driver of dynamic compression research is the quest to probe the pathways and kinetics of phase transitions. One of the unanswered questions in physics is the time dependence of phase diagrams and how to model it. When a material is loaded dynamically through equilibrium phase boundaries, it is the kinetics that determines the real time expression of a phase transition. That in turn can play a significant role in the thermodynamic path that the material takes. The material's end state, in a shock event, may depend on the kinetics of the process that produced this end state. There exists a relationship between the kinetics of a phase transition, the mesoscale structure of a solid, and its constitutive properties. However, the role that kinetics of phase transitions play in a material's constitutive properties is not well understood. This lack of understanding is due to a lack of experimental data of direct, atomic-scale *in-situ* measurements of kinetics of transitions during shock events. While several dynamic x-ray diffraction (DXRD) studies have examined shock-driven phase transitions [1–6] and discussed aspects of kinetics [7–9], only a few studies exist that explicitly quantify the kinetics of a shock-driven transformation, using DXRD, i.e., extract quantitative percentages of crystalline phases from DXRD, as a function of shock event time [10–12].

In this Rapid Communication, we report the kinetics of shock-driven formation of the β phase of Zr metal at the atomic and nanosecond scale. We present real-time tracking of a measurable quantity—the phase percentage of β-Zr—measured with DXRD, as the shock process unfolds over tens of nanoseconds. We establish a quantified expression of kinetics of formation of β-Zr under shock loading: transition incubation time, completion time, and crystallization rate. Probing kinetics experimentally can be hindered by gradients of stress and temperature that can develop under conventional shock loading. Here we uniquely make use—in combination with DXRD—of a multiple shock-and-release (mSR) loading pathway culminating in a quasisteady pressure (P) and temperature (T) state. Through a combination of DXRD and mSR loading we observe the nanosecond, atomic-scale response of the structure of Zr in the quasisteady state created as a result of impact and shock wave reverberation.

Zirconium has fascinated the high pressure community since Bridgman discovered the ω phase in 1952 (Fig. 1) [13]. Prior works examined the α (hcp) $\rightarrow$ ω (hexagonal) transition under static and dynamic compression [14–20], deformation under pressure [21], under shock compression [22–25], the phase boundaries [26,27], and the melt line [28]. Although first reported in 1990, the $\omega \rightarrow \beta$ (cubic) transition [29] is less studied [16,30,31]. We use *in situ* time-resolved synchrotron DXRD and photonic Doppler velocimetry (PDV [32], Fig. 2), and we monitor the kinetics of a shock-driven transition in Zr at nanosecond timescales (Fig. 3). Shock experiments are performed at the Dynamic Compression Sector at the Advanced Photon Source (APS) using a two-stage light gas gun. We expose Zr to a multistep dynamic loading pathway or mSR: firstly, shock compression to a Hugoniot state into the β phase (stage 1 in Fig. 1), secondly a multistep shock and release (stage 2 in Fig. 1) that culminates in a quasisteady state P/T near the β/ω phase boundary (stage 3 in Fig. 1). The final P/T state in the sample is defined by the intersection of the Lexan and TPX Hugoniots and remains relatively steady for the duration of the experiment [33,34].

We use a 23 keV pink x-ray beam for time-resolved (interval 153 ns), single-pulse DXRD (100 ps) and a two-image

*pekalit@sandia.gov; mullites@gmail.com

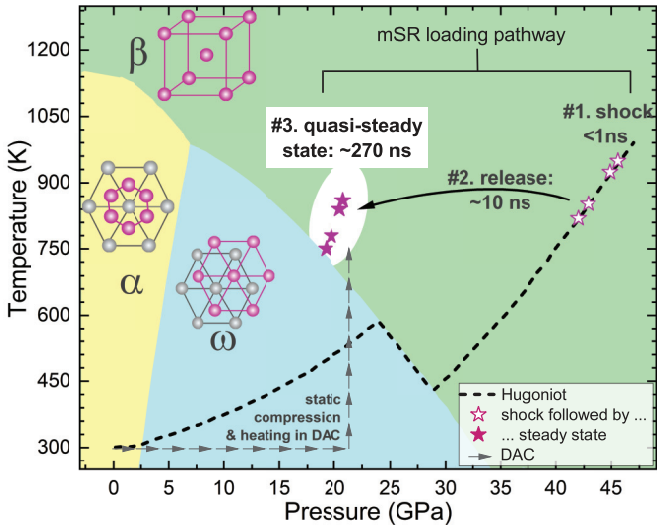

FIG. 1. The phase diagram of Zr, the Hugoniot [27], and the three stages of our dynamic mSR experiments: shock compression (#1—hollow stars), the release (#2—long arrow), and the steady P and T state, where we probe the kinetics of formation of β-Zr (#3—solid stars). A line of arrows marks the path of static compression and heating in DAC, culminating in the same P-T region as the mSR experiments.

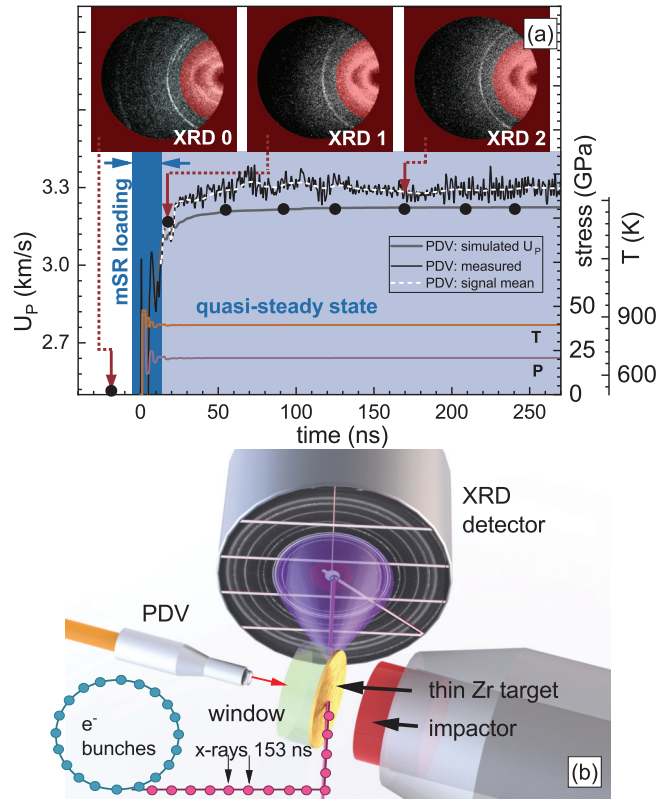

FIG. 2. Our multiple shock-and-release (mSR) experiment: (a) the measured PDV, modelled PDV, and modelled P and T state (see Supplemental Material [33]) and (b) geometry of time-resolved synchrotron DXRD. The PDV signals illustrate the stages of our experiment: the dynamic loading (dark blue, ~10 ns) and the quasisteady P-T state (light blue, ~250 ns). Black dots mark time stamps of DXRD patterns. Insets show example DXRD images of Debye rings.

XRD detector to study the temporal evolution of Zr structure during mSR compression. Based on DXRD we quantify the kinetics of formation of β-Zr and offer a kinetics' model (Fig. 4). Finally, we take Zr to the same thermodynamic end- state as in mSR but through a static compression and heating path using a diamond anvil cell (DAC) and 33 keV synchrotron XRD at the HPCAT beamline, APS (Figs. 1 and 3). We use the Zr structures extracted from our XRD DAC data as starting points in the analysis of mSR DXRD data. Experimental details and P-T modeling are in the Supplemental Material [33].

Dynamic vs static compression. A schematic of the mSR and DXRD configuration is in Fig. 2(b). In the first stage of the experiment, the Lexan® impactor generates a planar shock that produces a 42 ~ 46 GPa stress state on the Hugoniot. When the shock wave reaches the lower-impedance TPX® window, a release wave reflects from the interface and travels back into Zr. Subsequent release waves (sample/window) and shock waves (impactor/sample) are quasi-isentropic in their effect on the material. The shock and release waves continue to reverberate between the impactor and the window until all three—impactor, sample, window—are in P and T equilibrium. Because of the thin sample ~10 μm, reverberations result in the onset of a steady state, ~10 ns after impact. The steady P and T state is at 19 ~ 21 GPa and 750 ~ 860 °C, depending on shot, and persists for ~250 ns (Fig. 2(a) and Fig. S1 in Ref. [33]), which is the time interval before any edge waves or release fans from the TPX® free surface reach the sample. We note that with the mSR loading path we are able to probe a region of the phase diagram not accessible in a simple on-Hugoniot event. During our mSR experiments—illustrated by the PDV signal [Fig. 2(a)]—we acquire a DXRD pattern prior to impact, $t = 0$, and two more real-time *in situ* DXRD patterns after impact, separated by 153 ns, which is the time structure of the x-ray bunches [see time of Debye rings in Fig. 2(a)]. By repeating the same experiment we obtain a series of time-resolved DXRD patterns that allow us to track the unfolding of a phase transition in Zr throughout the mSR experiment. Figure 3 compares the pre-shot DXRD and DXRD for Zr quasi-isentropically released to the steady state of ~21 GPa and ~860 °C at two different times after impact: 15 ns and 168 ns.

To contrast our shock studies, we also examine phase transformations along a thermodynamic path that first takes Zr through static compression in DAC to ~22 GPa and adds heating up to ~940 °C, culminating in a similar P-T range as our mSR experiment (Fig. 1). Selected XRD patterns in DAC are presented together with results of Rietveld [35] refinements in Figs. 3(d)–3(f). On "cold" compression in DAC, we observe the $\alpha \rightarrow \omega$ transition (Fig. 1) [36,37]. At P and T values approaching those of the dynamic mSR compression, Zr goes from the low-symmetry ω (hexagonal) to a high symmetry β (cubic) structure in a first-order transition [Figs. 3(e)–3(f)] [29]. Some untransformed ω-Zr and minimal untransformed α-Zr are also present. From Rietveld refinements of static XRD DAC data we extract α, ω, and β-Zr structures at P and

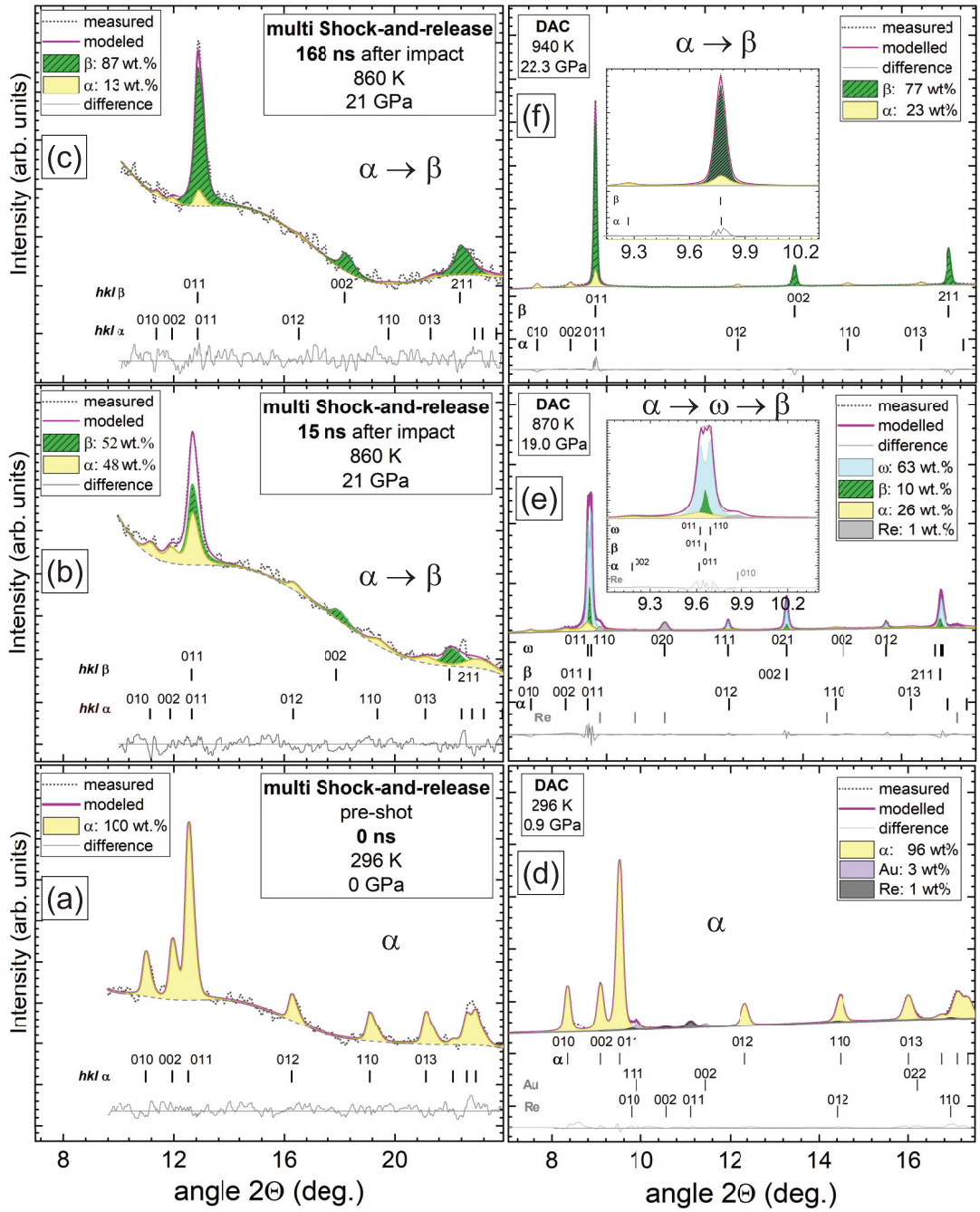

FIG. 3. Selected *in situ* time-resolved DXRD patterns of (a)–(c) mSR dynamic compression with the pre-shot at $t = 0$ and quasisteady state at $t = 15$ ns and $t = 168$ ns after impact, and (d)–(f) XRD of static compression in DAC. Overlapped are the measured and modeled patterns, the background and Miller indices for each phase. DXRD phase fraction errors are in Fig. 4(a). The path of static compression and heating in DAC (d)–(f) culminates in the *P*-*T* region where diffraction of the mSR experiments is measured (b),(c). We use the Zr structures extracted from XRD DAC data as starting points in the Rietveld analysis of DXRD. Re and Au are reflections from the gasket and the pressure standard, respectively.

T conditions close to those of our dynamic mSR experiments. We use those structures as starting models in the Rietveld analysis of our DXRD mSR results.

In mSR experiments, after shock compression, we track the structure of Zr through ~250 ns of the steady state [Figs. 3(b) and 3(c)]. Rietveld refinements indicate that under shock compression and quasi-isentropic reverberation to ~21 GPa and ~860 °C, Zr undergoes a direct $\alpha \rightarrow \beta$ phase transition. Over the duration of steady state, we observe the x-ray unit cell volume decrease in time consistent with the observed decreasing velocity from the PDV [33]. Recently, two works reported contradictory findings on a laser-shock-driven phase transition at ~20 GPa in Zr. One ascribed it to an $\alpha \rightarrow \omega$ [8] and the other to an $\alpha \rightarrow \beta$ transition [38]. Both works were

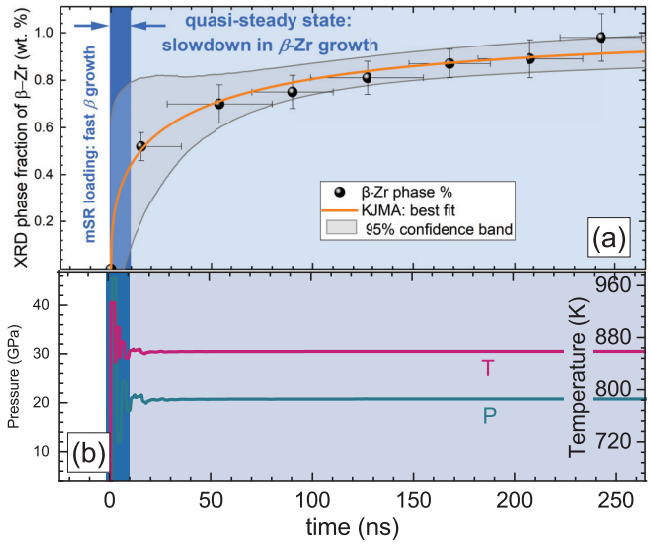

FIG. 4. Kinetics of formation of β-Zr over ~250 ns. (a) Quantitative analysis of the evolution of β-Zr phase fraction from our analysis of time-resolved DXRD. Error bars are two standard deviations. The fit of KJMA kinetics model is shown in orange. The short incubation time and the long time needed to complete the transition show that atomic displacement during the transition requires tens of ns to complete. (b) Modeled time evolution of P and T in Zr, along the path of the x-ray beam, illustrating the two stages of our mSR experiment: dynamic loading (dark-blue window, ~10 ns) and the steady P-T state (light-blue window, ~250 ns).

qualitative and neither used quantitative XRD analysis. In both works Zr was subjected to a large distribution of stresses hence a comparison with our work is not possible.

Quantifying the kinetics of the shock-driven phase transition. Our mSR loading is ideal for monitoring the kinetics of structural changes in Zr: The shock wave reverberations quickly lead to the onset of a quasisteady P-T state, which persists for ~250 ns after shock. In this state, in the absence of thermodynamic gradients along the path of the x-ray probe, the observed evolution in DXRD patterns can only originate from structural transformations occurring in the shock-loaded Zr. We perform quantitative analysis of the kinetics of formation of β-Zr phase in the steady state for all data of our mSR experiments. We treat all shots at stresses between 19 and 21 GPa as equivalent, because the calculated T differences are at most ~110 K (Table S1 in Ref. [33]). Figure 4(a) shows the increase in phase fraction of β-Zr in the steady state during ~250 ns, obtained from Rietveld refinements of our DXRD patterns. To quantify the kinetics of the Zr transition—in the absence of a dedicated model for shock-driven processes—we use the nucleation model developed by Kolmogorov [39], Johnson and Mehl [40], and Avrami [41–43] (KJMA), but we apply it to nanosecond processes [11,12]. Using the KJMA formalism, the time-dependent phase fraction of β-Zr(t) is given by:

$$\beta(t) = 1 - \exp(-(k(t-\tau))^N). \quad (1)$$

τ is the incubation time of the transition and k is the crystallization rate constant. The Avrami parameter N can be indicative of nucleation mechanisms [44,45]. The best fit to our data and the confidence interval (CI) representing the 0.025 and 0.975 quantiles yield: $\tau = 0$ ns (CI: 0-29.6), $N = 0.445$ (CI: 0.128-0.671), and $k = 0.030$ 1/ns (CI: 0.017–0.50). This fit suggests a transition characterized by an incubation time $\tau \sim 0$ ns. The short incubation time together with the ~250 ns needed to complete the transition are consistent with first-order martensitic kinetics, and the atomic displacement during transition requires tens of nanoseconds to complete the process. The applicability of the KJMA formalism for describing polymorphic transitions under shock compression must be approached carefully, since it was developed for transformations between isotropic phases with a small volume jump and a zero shear modulus. While the initial loading path over the first ~10 ns is likely to affect the kinetics rate, we chose to understand the long-time kinetics as the Zr sits in a quasisteady P-T state, using the KJMA phenomenological model. Although imperfect, this model does provide insight into the transition incubation time and rate for this dynamic loading path.

To give perspective on the broader implications of our results, it is valuable to reflect on why the quantification of kinetics of phase transitions is so important. Shock physics centers on understanding the behavior of materials subjected to shock-inducing pressure waves and on probing material properties well away from ambient conditions. Dynamic loading can drive phase transitions and allow for probing phase boundaries throughout the P-T space. Phase transitions are accompanied by changes in constitutive properties and transport properties. Since these processes are dynamically driven, often with large strain rates, the experimental signatures of a phase transition may not correspond to the true equilibrium phase boundary. This is because the completion of the transition is subject to the underlying kinetics. A kinetically delayed transition may require the material to be substantially "overdriven" before the transition occurs, resulting in a different end state, compared with a transition without any delay due to kinetics. More broadly the transition kinetics can play a significant role in the thermodynamic path that the material takes, along with all derived properties associated with the new phase.

In summary, in this work we demonstrate that under dynamic compression to ~21 GPa and ~860 K, Zr undergoes an $\alpha \rightarrow \beta$ phase transition. We quantify the kinetics of formation of β-Zr phase at the atomic scale, by uniquely combining time-resolved synchrotron DXRD with a multiple shock-and-release loading experiment. We track the entire phase transition process, from incubation to completion. We provide critical quantitative data that will allow to validate theoretical models of transition kinetics: incubation time, completion time and crystallization rate. The results of our work are relevant not only to Zr but also to other group 4 elements, and in particular to the behavior of Ti under high pressure [46,47]. Access to data of kinetics of transformation, such as the one in this work, shows the true time expression of a dynamically-driven phase transition and highlights the time dependence of phase diagrams.

The authors are grateful to Dr. T. R. Mattsson, SNL, for a critical reading of the paper and valuable advice. The authors thank Dr. M. P. Desjarlais, SNL for enlightening discussions.

The authors are grateful to Dr. D. H. Dolan, SNL for valuable discussion on PDV and the intricacies of reverberation experiments and to Dr. M. A. Rodriguez, SNL for valuable discussions on the Rietveld technique. Sandia National Laboratories is a multimission laboratory managed and operated by National Technology and Engineering Solutions of Sandia, LLC., a wholly owned subsidiary of Honeywell International, Inc., for the US Department of Energy's National Nuclear Security Administration under Contract No. DE-NA-0003525. This paper describes objective technical results and analysis. Any subjective views or opinions that might be expressed in the paper do not necessarily represent the views of the US Department of Energy or the United States Government. A portion of this publication is based upon work performed at the Dynamic Compression Sector, which is operated by Washington State University under the US Department of Energy (DOE)/National Nuclear Security Administration Award No. DE-NA0002442. Portions of this work were performed at HPCAT (Sector 16), Advanced Photon Source (APS), Argonne National Laboratory. HPCAT operations are supported by DOE-NNSA's Office of Experimental Sciences. The Advanced Photon Source is a U.S. Department of Energy (DOE) Office of Science User Facility operated for the DOE Office of Science by Argonne National Laboratory under Contract No. DE-AC02-06CH11357. The authors thank P. Rigg, N. Sinclair, A. Schuman, and the DCS user facility team as well as E. Rod, C. Benson, and the HPCAT user facility team for technical assistance. M.W. acknowledges support from the National Nuclear Security Administration under the Stewardship Science Academic Alliances program through DOE Cooperative Agreement No. DE-283 NA0001982. P.K. is grateful to S. Payne of MSTS and to N. Cofer, L. Pacheco, J. Usher, K. Hodge, and R. Hickman of SNL for invaluable assistance with preparing the experiments. C. Blada and M. Schollmeier of SNL created the fabulous rendering of the dynamic XRD experimental setup.

[1] K. Ichiyanagi and K. G. Nakamura, Metals **6**, 17 (2016).
[2] S. J. Turneaure, N. Sinclair, and Y. M. Gupta, Phys. Rev. Lett. **117**, 045502 (2016).
[3] S. J. Turneaure, S. M. Sharma, T. J. Volz, J. M. Winey, and Y. M. Gupta, Sci. Adv. **3**, eaao3561 (2017).
[4] D. Kraus, A. Ravasio, M. Gauthier, D. O. Gericke, J. Vorberger, S. Frydrych, J. Helfrich, L. B. Fletcher, G. Schaumann, B. Nagler, B. Barbrel, B. Bachmann, E. J. Gamboa, S. Gode, E. Granados, G. Gregori, H. J. Lee, P. Neumayer, W. Schumaker, T. Döppner, R. W. Falcone, S. H. Glenzer, and M. Roth, Nat. Commun. **7**, 10970 (2016).
[5] D. H. Kalantar, J. F. Belak, G. W. Collins, J. D. Colvin, H. M. Davies, J. H. Eggert, T. C. Germann, J. Hawreliak, B. L. Holian, K. Kadau, P. S. Lomdahl, H. E. Lorenzana, M. A. Meyers, K. Rosolankova, M. S. Schneider, J. Sheppard, J. S. Stolken, and J. S. Wark, Phys. Rev. Lett. **95**, 075502 (2005).
[6] M. Millot, F. Coppari, J. R. Rygg, A. C. Barrios, S. Hamel, D. C. Swift, and J. H. Eggert, Nature (London) **569**, 251 (2019).
[7] C. E. Wehrenberg, A. J. Comley, N. R. Barton, F. Coppari, D. Fratanduono, C. M. Huntington, B. R. Maddox, H. S. Park, C. Plechaty, S. T. Prisbrey, B. A. Remington, and R. E. Rudd, Phys. Rev. B **92**, 104305 (2015).
[8] T. D. Swinburne, M. G. Glavicic, K. M. Rahman, N. G. Jones, J. Coakley, D. E. Eakins, T. G. White, V. Tong, D. Milathianaki, G. J. Williams, D. Rugg, A. P. Sutton, and D. Dye, Phys. Rev. B **93**, 144119 (2016).
[9] C. M. Pepin, A. Sollier, A. Marizy, F. Occelli, M. Sander, R. Torchio, and P. Loubeyre, Phys. Rev. B **100**, 060101(R) (2019).
[10] A. E. Gleason, C. A. Bolme, H. J. Lee, B. Nagler, E. Galtier, D. Milathianaki, J. Hawreliak, R. G. Kraus, J. H. Eggert, D. E. Fratanduono, G. W. Collins, R. Sandberg, W. Yang, and W. L. Mao, Nat. Commun. **6**, 8191 (2015).
[11] A. E. Gleason, C. A. Bolme, E. Galtier, H. J. Lee, E. Granados, D. H. Dolan, C. T. Seagle, T. Ao, S. Ali, A. Lazicki, D. Swift, P. Celliers, and W. L. Mao, Phys. Rev. Lett. **119**, 025701 (2017).
[12] P. Kalita, P. Specht, S. Root, N. Sinclair, A. Schuman, M. White, A. L. Cornelius, J. Smith, and S. Sinogeikin, Phys. Rev. Lett. **119**, 255701 (2017).
[13] P. W. Bridgman, Proc. Am. Acad. Arts Sci. **81**, 165 (1952).
[14] J. C. Jamieson, Science **140**, 72 (1963).
[15] M. P. Usikov and V. A. Zilbershtein, Phys. Status Solidi A **19**, 53 (1973).
[16] J. Z. Zhang, Y. S. Zhao, C. Pantea, J. Qian, L. L. Daemen, P. A. Rigg, R. S. Hixson, C. W. Greeff, G. T. Gray, Y. P. Yang, L. P. Wang, Y. B. Wang, and T. Uchida, J. Phys. Chem. Solids **66**, 1213 (2005).
[17] H. R. Wenk, P. Kaercher, W. Kanitpanyacharoen, E. Zepeda-Alarcon, and Y. Wang, Phys. Rev. Lett. **111**, 195701 (2013).
[18] M. K. Jacobsen, N. Velisavljevic, and S. V. Sinogeikin, J. Appl. Phys. **118**, 025902 (2015).
[19] A. Dewaele, R. André, F. Occelli, O. Mathon, S. Pascarelli, T. Irifune, and P. Loubeyre, High Press. Res. **36**, 237 (2016).
[20] S. H. Guan and Z. P. Liu, Phys. Chem. Chem. Phys. **18**, 4527 (2016).
[21] A. A. Yaroslavzev, I. A. Evdokimov, B. A. Kulnitskiy, I. A. Perezhogin, V. D. Blank, I. V. Pakhomov, and V. V. Denisov, Mater. Res. Express **6**, 046506 (2019).
[22] A. R. Kutsar, V. N. German, and G. I. Nosova, Dokl. Akad. Nauk SSSR **213**, 81 (1973).
[23] G. Jyoti, K. D. Joshi, S. C. Gupta, S. K. Sikka, G. K. Dey, and S. Banerjee, Shock Compression of Condensed Matter **370**, 227 (1996).
[24] H. X. Zong, T. Lookman, X. D. Ding, C. Nisoli, D. Brown, S. R. Niezgoda, and S. Jun, Acta Mater. **77**, 191 (2014).
[25] E. K. Cerreta, G. T. Gray III, C. P. Trujillo, D. W. Brown, and C. N. Tome, in *Shock Compression of Condensed Matter-2007*, edited by M. Elert, M. D. Furnish, R. Chau, N. Holmes, and J. Nguyen (AIP, Melville, NY, 2007), p. 635.
[26] A. Jayaraman, W. Klement, and G. C. Kennedy, Phys. Rev. **131**, 644 (1963).
[27] C. W. Greeff, Modell. Simul. Mater. Sci. Eng. **13**, 1015 (2005).
[28] P. Parisiades, F. Cova, and G. Garbarino, Phys. Rev. B **100**, 054102 (2019).
[29] H. Xia, S. J. Duclos, A. L. Ruoff, and Y. K. Vohra, Phys. Rev. Lett. **64**, 204 (1990).

[30] M. T. Perez-Prado and A. P. Zhilyaev, Phys. Rev. Lett. **102**, 175504 (2009).
[31] H. B. Radousky, M. R. Armstrong, R. A. Austin, E. Stavrou, S. Brown, A. A. Chernov, A. E. Gleason, E. Granados, P. Grivickas, N. Holtgrewe, H. J. Lee, S. S. Lobanov, B. Nagler, I. Nam, V. Prakapenka, C. Prescher, P. Walter, A. F. Goncharov, and J. L. Belof, Phys. Rev. Research **2**, 013192 (2020).
[32] O. T. Strand, D. R. Goosman, C. Martinez, T. L. Whitworth, and W. W. Kuhlow, Rev. Sci. Instrum. **77**, 083108 (2006).
[33] See Supplemental Material at http://link.aps.org/supplemental/10.1103/PhysRevB.102.060101, which include shock experiment details, static compression experiment details, methods used to analyze velocimetry results, modeling of shock pressure and temperature, and modeling of kinetics and includes Refs. [11,12,18,27,29,32,44,48–60].
[34] D. H. Dolan and Y. M. Gupta, J. Chem. Phys. **121**, 9050 (2004).
[35] H. M. Rietveld, J. Appl. Crystallogr. **2**, 65 (1969).
[36] N. Velisavljevic, G. N. Chesnut, L. L. Stevens, and D. M. Dattelbaum, J. Phys.: Condens. Matter **23**, 125402 (2011).
[37] T. Hattori, H. Saito, H. Kaneko, Y. Okajima, K. Aoki, and W. Utsumi, Phys. Rev. Lett. **96**, 255504 (2006).
[38] M. R. Armstrong, H. B. Radousky, R. A. Austin, E. Stavrou, H. Zong, G. J. Ackland, S. Brown, J. C. Crowhurst, A. E. Gleason, E. Granados, P. Grivickas, N. Holtgrewe, H. J. Lee, T. T. Li, S. Lobanov, J. T. McKeown, R. Nagler, I. Nam, A. J. Nelson, V. Prakapenka, C. Prescher, J. D. Roehling, N. E. Teslich, P. Walter, A. F. Goncharov, and J. L. Belof, arXiv:1808.02181.
[39] A. Kolmogorov, Bull. Acad. Sci. USSR Phys. Ser. **3**, 555 (1937).
[40] W. Johnson and R. Mehl, Trans. Am. Inst. Min., Metall. Pet. Eng. **135**, 416 (1939).
[41] M. Avrami, J. Chem. Phys. **7**, 1103 (1939).
[42] M. Avrami, J. Chem. Phys. **8**, 212 (1940).
[43] M. Avrami, J. Chem. Phys. **9**, 177 (1941).
[44] J. W. Cahn, Acta Metall. **4**, 449 (1956).
[45] A. K. Singh, Bull. Mater. Sci. **5**, 219 (1983).
[46] D. Errandonea, Y. Meng, M. Somayazulu, and D. Hausermann, Physica B-Condensed Matter **355**, 116 (2005).
[47] L. Gao, X. Ding, T. Lookman, J. Sun, and E. K. H. Salje, Appl. Phys. Lett. **109**, 031912 (2016).
[48] S. Root, T. R. Mattsson, K. Cochrane, R. W. Lemke, and M. D. Knudson, J. Appl. Phys. **118**, 205901 (2015).
[49] C. Prescher and V. B. Prakapenka, High Pressure Res. **35**, 223 (2015).
[50] T. Ao and D. H. Dolan, SIRHEN: A data reduction program for photonic Doppler velocimetry measurements, Report No. SAND2010-3628 (Sandia National Laboratories, 2010).
[51] O. L. Anderson, D. G. Isaak, and S. Yamamoto, J. Appl. Phys. **65**, 1534 (1989).
[52] J. A. Lopes-Da-Silva and J. A. P. Coutinho, Energy & Fuels **21**, 3612 (2007).
[53] W. Carter and S. Marsh, Hugoniot Equation of State of Polymers, Report No. LA-13006-MS (Los Alamos National Laboratory, 1995).
[54] S. Root, R. J. Magyar, J. H. Carpenter, D. L. Hanson, and T. R. Mattsson, Phys. Rev. Lett. **105**, 085501 (2010).
[55] W. G. Burgers, Physica **1**, 561 (1934).
[56] Y. K. Vohra, Acta Metall. **27**, 1671 (1979).
[57] N. X. Sun, X. D. Liu, and K. Lu, Scr. Mater. **34**, 1201 (1996).
[58] N. V. Chandra Shekar and K. G. Rajan, Bull. Mater. Sci. **24**, 1 (2001).
[59] A. K. Singh, C. Divakar, and M. Mohan, Rev. Sci. Instrum. **54**, 1407 (1983).
[60] A. K. Singh, M. Mohan, and C. Divakar, J. Appl. Phys. **54**, 5721 (1983).